*Bull. Mater. Sci.* (2021)44:152
https://doi.org/10.1007/s12034-021-02431-4



# Target phase-induced compositional control in liquid-phase pulsed laser ablation produced titanium ferrite nanomaterials

**ABHISHEK SHUKLA[1,2], SUBHASH C SINGH[1,2,3,*], R K KOTNALA[4], K N UTTAM[1], CHUNLEI GUO[3] and R GOPAL[1]**

[1]Laser Spectroscopy and Nanomaterials Lab, Physics Department, University of Allahabad, Allahabad 211002, India
[2]Changchun Institute of Optics, Fine Mechanics and Physics, Changchun 130033, China
[3]The Institute of Optics, University of Rochester, Rochester, NY 14627, USA
[4]Magnetic and Multiferroic, National Physical Laboratory (NPL), New Delhi 110012, India
*Author for correspondence (ssingh49@ur.rochester.edu)

MS received 25 June 2020; accepted 10 December 2020

**Abstract.** Titanium ferrite nanoparticles (NPs) are synthesized using liquid-phase pulsed laser ablation (LP-PLA) technique with two different lines of approaches for targets: the first target is the pellet made from the mixture of oxides of iron and titanium, while the second target is iron and titanium metal rods. In the second approach of metal rods, the titanium rod was first ablated in double-distilled water and then, the use of obtained colloidal solution of NPs as a medium for the ablation of iron rod. The titanium ferrite nanomaterials produced from these two types of targets are characterized using X-ray diffraction (XRD), ultraviolet–visible absorption spectroscopy (UV–Vis), attenuated total reflectance Fourier transform infrared spectroscopy (ATR-FTIR), Raman spectroscopy and vibrating sample magnetometer (VSM) measurements. XRD measurements show multiphase structure for as-produced titanium ferrite NPs. The structural, compositional, optical, bonding nature and magnetic properties of nanomaterials produced from two different targets under same experimental conditions are systematically studied. Comparatively higher yield, larger average particle size and smaller saturation magnetism are observed for nanomaterials produced from ablation of interface of metallic targets over the pellet made from the mixture of corresponding metal oxide powders. ATR-FTIR and Raman studies demonstrate synthesis of titanium–iron-oxide phase of titanium ferrite NPs. The results of present research demonstrate collision and intermixing of plasmas from two different species and can be used to produce ferrite NPs of other metals.

**Keywords.** Laser ablation; target compositions; titanium ferrite; magnetic nanomaterials.

## 1. Introduction

Recently, engineering and design for compositional control in ferrites, and single, bi- or tri-metallic oxide ferrites have attracted strong attention of researchers due to their composition-dependent structural, electronic, photocatalytic and optical applications [1–4]. For example, control of silver and gold ratio in Au–Ag alloy and copper to selenium ratio in $Cu_{2-x}Se$ nanoparticles (NPs) determines their surface plasmon resonance peak positions, thermoelectric and electronic properties [5,6]. Similarly, different physical, chemical, electronic and ferromagnetic properties of metal compound NPs rely on their cation to anion ratio. Metal ferrite ($M_xFe_{2-x}O_4$; M = Ti, Cr, Mn, Fe, Co, Ni, etc.) NPs have shown interesting magnetic, magneto-optical, magneto-thermal and magneto-resistive properties and have a wealth of applications in energy storage, sensing, separations and catalysis [7–12]. These properties of ferrite materials are governed by their elemental compositions. Active metal oxide, such as $TiO_2$ nanomaterials are widely used as a photocatalyst for water/air purification and fuel generation, for optoelectronic devices, for gas sensors, etc. [13–16], while $Fe_3O_4$ NPs have potential applications in spintronics, sensing, drug delivery, magnetic resonance imaging, contrast agent, photocatalysts, solar energy conversion and photoelectrochemical water splitting [17–22]. Combining electronic and optical properties of $TiO_2$ with ferromagnetic functionality of $Fe_3O_4$ would give birth to a new class of materials where magneto-electronic properties can be controlled via their elemental composition.

Generally, synthesis of alloy and ferrite NPs, uses multistep time-consuming chemical co-precipitation or solid-state chemistry approaches which either involve hazardous chemicals with negative impact on the environment or use high temperature. A simple, sustainable, fast and environmentally friendly approach is always required for processing of multi-elemental NPs. Liquid-phase pulsed laser ablation (LP-PLA) is a simple, one-step, one-pot and environmentally friendly green method, where laser-produced-plasmas (LPPs) of target material get strongly confined under liquid medium [23]. Strong confinement of LPPs produces high-temperature, high-pressure

Published online: 24 May 2021

and high-density conditions inside the plasma that initiate non-thermal-equilibrium condition inside the plasma and strong interaction between plasma and liquid at plasma–liquid interface. Over the past decade, LP-PLA has been successively used for the synthesis of highly stable colloidal solutions of bimetallic/trimetallic alloys and metal compound NPs, such as ZnO, $Cd(OH)_2$, ZnSe, PbTe, CdTe, GaAs, AuAg, PtAu, AgCu, AuFe, BiInSn and core@shell FeMn@$FeMn_2O_4$, Ag@Au, Cu@Au, CdSe, ZnTe NPs [23–38]. At a given laser pulse energy, nature and composition of the target determine temperature, pressure, density and composition of plasma and hence, size and composition of produced NPs [39]. Very recently, we reported LP-PLA synthesis of titanium ferrite NPs. The ratio of Ti and Fe in the produced NPs and thus, their magnetic properties was tuned by varying the composition of iron oxide and titanium oxide in the cold-pressed target [40].

Here, in this paper, we studied the effects of two different types of targets in the synthesis of multi-phasic titanium ferrite nanomaterials. In the first case, the target is made by compressing a mixture of iron oxide and titanium oxide, similar to our previous work [40], to make a hard pellet. However, in the second case, colloidal solution of titanium dioxide NPs was first prepared by laser ablation of titanium rod in the double-distilled water [41]. Later, the obtained colloidal solution of titanium dioxide NPs is used as a medium for the ablation of iron rod under the same experimental conditions. Mechanisms for the ablation of metals and ceramic powder samples are entirely different due to their different pathways for the absorption of laser pulse energy, nature and composition of laser-produced plasmas (LPPs), and reaction of corresponding LPPs with the surrounding medium to make plasma-induced plasmas (PIPs) [23]. In general, physical confinement of LPPs between solid target and surrounding liquid, increases its temperature, density and kinetic energy of plasma species. Higher free electron density in metals over those of ceramic powders provides larger absorption cross-section for the laser pulse that results higher rate of material ablation and hence, higher NPs yield and larger average particle size [23]. Moreover, due to its higher temperature, pressure and density, plasmas produced by metal ablation could have a higher degree of thermodynamic non-equilibrium, resulting a smaller time available for the interaction and mixing of LPPs from two different metals. A short interaction time between two plasmas and strong thermodynamic non-equilibrium could create several defects in the lattice that reduces saturation ferromagnetism in nanomaterials produced from metals as compared to those produced from mixture of powder. On the other hand, lower temperature and pressure inside LPPs produced from pellet ablation set a better thermal equilibrium for reaction between two plasmas to produce higher quality of spinel ferrite nanocrystals with comparatively smaller size.

## 2. Synthesis and characterization

The schematic of LP-PLA for the synthesis of titanium ferrite NPs is shown in figure 1. In the first route: iron oxide ($Fe_2O_3$: 1.6 g) and titanium dioxide ($TiO_2$: 40 mg) (purity 99.999%, Sigma-Aldrich) powders were mixed homogeneously, pelletized through cold-pressing and annealed at 1000°C to make a target for ablation. In the second route, metal rods of titanium and iron (99.99%, Specpure, Johnston Mathey, UK) were used as target for producing titanium ferrite NPs. Experimental arrangement and procedure are similar to our previous work [3,35,40,41]. Briefly, fundamental output (1064 nm) from a pulsed Nd-YAG laser (Spectra Physics, Quanta-Ray, USA) operating at 50 mJ per pulse energy, 10 ns pulse width and 10 Hz repetition rate was focussed on the surface of target (pellet/rod) securely attached at the bottom of a glass vessel containing doubled-distilled water. Double-distilled water was used to avoid undesired contamination of NPs or undesired doping of NPs with ions present in tap water. The laser beam was focussed to the spot size of ~200 μm at the target surface resulting in ~159 J $cm^{-2}$ of power density. For the first case: the pellet made from the mixture of iron oxide and titanium oxide powders was ablated for 60 min. For the second case: titanium rod was ablated in double-distilled water for 60 min to produce a colloidal solution of titanium dioxide NPs [41]. Thus, produced colloidal solution of titanium dioxide NPs was used as medium for the ablation of iron rod for next 60 min. All other ablation parameters remain unchanged for both cases. PerkinElmer Lambda-35 double beam spectrophotometer was used to measure UV–Vis

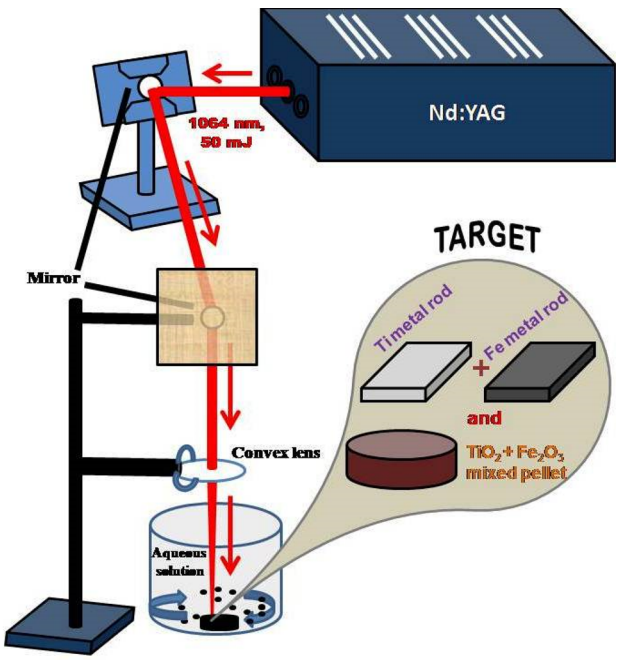


**Figure 1.** Experimental setup used for the synthesis of titanium ferrite nanoparticles by laser ablation method.

absorption of as-obtained colloidal solution of NPs. NP samples obtained after evaporating water were used for its structural characterization using CuKα line ($\lambda$ = 1.5406 Å) from Philips X'PERT X-ray diffractometer. Lakeshore vibrating sample magnetometer was used for magnetic measurement of as-obtained dried powders. Attenuated total reflectance Fourier transform infrared (ATR-FTIR) spectra of powder samples were recorded using ABB Bomen-FTIR spectrometer, while Raman measurements were performed using UniRAM Micro Raman spectrometer equipped with 785 nm excitation laser and BX3 microscope system.

## 3. Results and discussion

### 3.1 *Crystallographic and compositional investigation of NPs produced from LP-PLA of oxide pellet and metal rods*

X-ray diffraction (XRD) measurement is used to study the crystalline structure and composition of as-produced magnetic materials. The crystalline content, crystalline phases, spacing between lattice planes, preferential order and epitaxial growth of nanocrystals were analysed. Since each material has its unique diffraction pattern so, materials and compounds can be identified using a database of diffraction pattern. The XRD patterns of titanium ferrite NPs obtained through ablation of pellet and rods in double-distilled water are presented in figure 2. From these measurements, one can see that the product obtained through LP-PLA of pellet has multiphase of titanium ferrite including $TiFe_2O_4$, $Ti_3Fe_3O$, $TiFe_2O_5$ and $Fe_{0.23}(Fe_{1.95}Ti_{0.42})O_4$ [42]. Few XRD peaks, assigned to $Fe_2O_3$, are due to the presence of non-reacted iron oxide from the mother target. Similar to the pellet target, PLA of iron rod in the colloidal solution of titanium dioxide NPs also produces mixture of different phases of titanium ferrite including $Ti_2Fe_2O_7$ (landauite), $TiFe_2O_5$ (pseudobrookite) and $(Ti_{0.81}Fe_{0.13})O_{1.92}$ along with iron-deficient wuestile phase of iron oxide $(Fe_{0.87}O)_{10}$. From these XRD investigations, one can see that NPs produced with PLA of pellet has much wider peak width (FWHM) as compared to that produced with PLA of rods. The wider widths of XRD peaks from NPs produced with LP-PLA of pellets show their smaller crystalline size over that produced with LP-PLA of rods under same experimental conditions. It can be noticed here that pseudobrookite phase, one of the important structures of titanium ferrite [43], is produced with LP-PLA of both types of targets (table 1). The crystalline size of NPs is calculated from XRD peaks using Scherrer's formula presented as follows:

$$D = \frac{K\lambda}{\beta \cos\theta},$$

where the constant $K = 0.97$, $\lambda = 1.5406$ Å is the wavelength of X-ray line used and $\beta$ is the full width at half maximum (FWHM). The average crystalline size is estimated using five most intense peaks of each sample. The crystalline size of titanium ferrite NPs obtained from the ablation of pellet is ~23 nm, while that produced with the PLA of rods is ~50 nm. Larger crystalline size of NPs produced from LP-PLA of metal rod as compared to that of ceramic pellet is possibly related with higher rate of ablation and hence, material removal from metals as compared to the ceramic. Metal has much higher free electron density over metal oxide that facilitates higher absorption of laser energy by metal rods and hence, higher rate of material removal. Larger amount of available atoms/ion in the material ablated from target, generally provides larger size of clusters/particles [44–46].

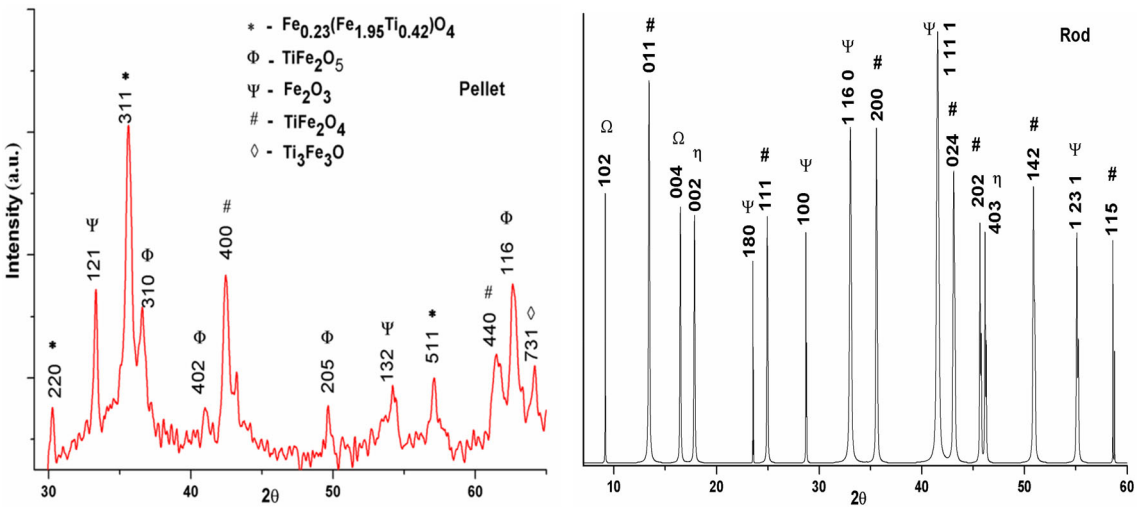


**Figure 2.** XRD peaks of titanium ferrite nanoparticles obtained in pellet and rod routes. (In second figure symbols: 'Ω' - $Fe_{0.87}O_{10}$ (wuestile), '#' - $Ti_2Fe_2O_7$ (landauite), 'η' - $TiFe_2O_5$ (pseudobrookite), 'Ψ' - $Ti_{0.81}Fe_{0.13}O_{1.92}$ (non-ambient temperature).

**Table 1.** Comparison of XRD data between the pellet and rod.

| Pellet | | Rod | |
|---|---|---|---|
| Formula/mineral name | JCPDS no. | Formula/mineral name | JCPDS no. |
| $Fe_{0.23}(Fe_{1.95}Ti_{0.42})O_4$ (titanomaghemite) | 84-1595 | $Fe_{0.87}O_{10}$ (wuestile) | 71-0161 |
| $TiFe_2O_5$ (pseudobrookite) | 73-1631 | $Ti_2Fe_2O_7$ (landauite) | 72-2325 |
| $Fe_2O_3$ (hematite) | 85-0599 | $TiFe_2O_5$ (pseudobrookite) | 76-1743 |
| $TiFe_2O_4$ (ulvoespinel) | 71-1141 | $Ti_{0.81}Fe_{0.13}O_{1.92}$ (non-ambient temperature) | 70-0143 |
| $Ti_3Fe_3O$ | 75-0397 | | |

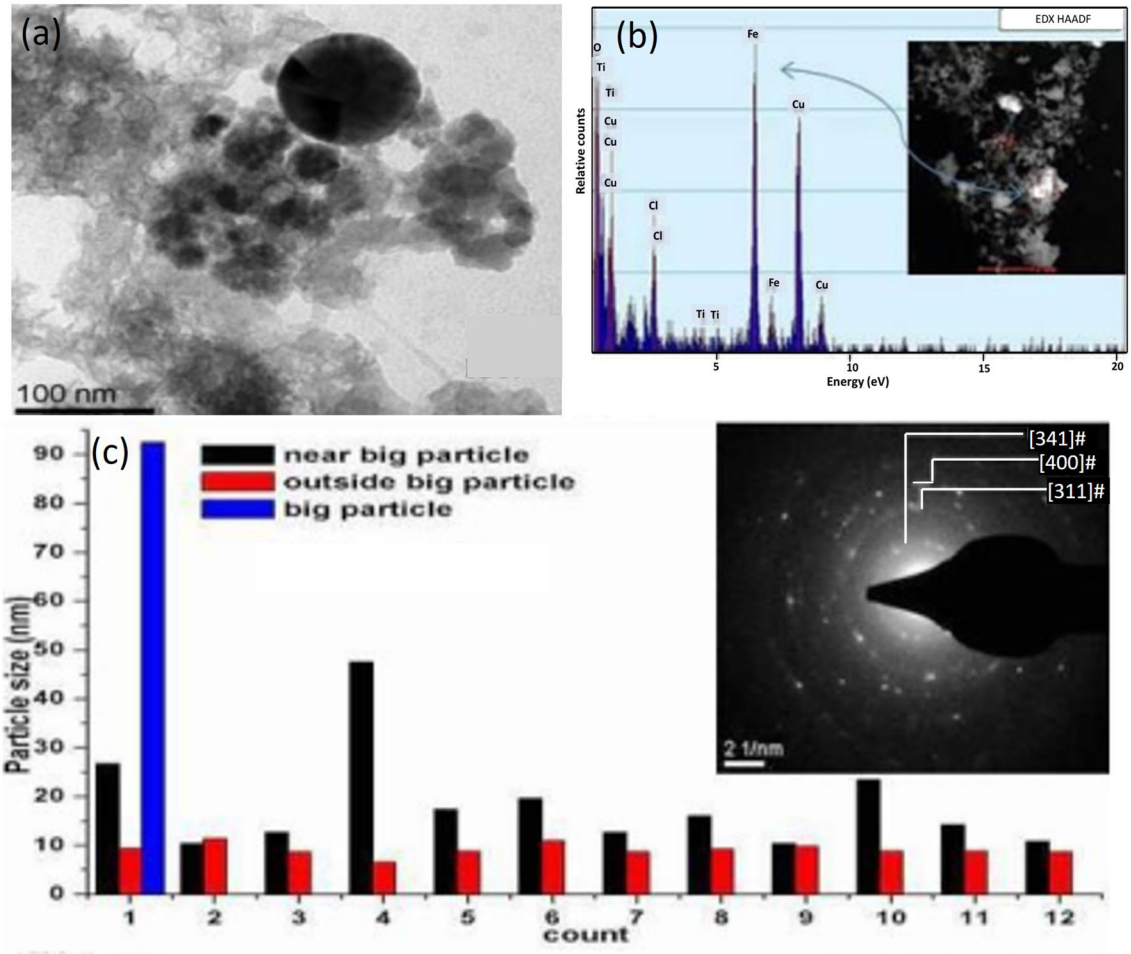


**Figure 3.** (**a**) Transmission electron microscopic (TEM) image, (**b**) EDAX spectrum, and (**c**) particle size histogram and selective area diffraction pattern (inset) of titanium ferrite NPs produced from pellet.

### 3.2 *TEM imaging and EDAX spectroscopy*

The transmission electron microscopy (TEM) image of NPs produced from pellet, as a target, in the LP-PLA is shown in figure 3a. From the image, we can see that NPs are in the size range of 10–90 nm. There is a big particle of ~90 nm diameter. Close to the big particle, there are NPs in the size range of 15–48 nm (shown with black bar in figure 3c). The energy dispersive X-ray absorption (EDAX) spectrum of NPs shows Fe, Ti and O from titanium ferrite and Cu from the grid. The bright spots in the selective area diffraction pattern (SEAD) shows high crystallinity of as-produced titanium ferrite NPs (inset: figure 3c).

### 3.3 *Optical properties of titanium ferrite NPs produced by LP-PLA*

UV–Vis absorption spectroscopy is a useful tool to determine relative density of particles in the solution,

determination in size and band gap energy of particles, and growth or size reduction dynamics of NPs [44]. The UV–Vis absorption spectra of as-synthesized colloidal solution of titanium ferrite NPs produced by two approaches are presented in figure 4. The UV–visible absorption spectra of bulk $Fe_2O_3$ (figure 4a, black curve) and bulk $TiO_2$ (figure 4a, red curve) powders, ultrasonically dispersed in double-distilled water, show their characteristic band-edge absorption peaks in visible and UV spectral regions, respectively. The broad absorption peak of iron oxide dispersion ranging from 300 to 650 nm with hump at 580 nm, shows larger-sized particles with broad size distribution. The colloidal solution of NPs produced by LP-PLA of pellet made from the mixture of 40 mg $TiO_2$ and 1.6 g $Fe_2O_3$ has absorption hump around 250 nm with long tail in the visible and NIR regions. Presence of absorption hump, for as-produced colloidal solution, in between the characteristic absorption peaks of $TiO_2$ and $Fe_2O_3$ shows synthesis of titanium ferrite NPs [40].

Optical absorption spectra of colloidal solution of NPs produced with LP-PLA of Ti (black curve) and Fe (red curve) rods in double-distilled water, and ablation of iron rod in the colloidal solution of NPs produced by ablation of titanium rod (blue curve) are shown in figure 4b. Experimental conditions for the ablation of titanium rod in water and characteristics (peak position and peak width) of UV–visible absorption of as-produced colloidal solution of NPs (black curve) are similar to our previous work [41]. Therefore, in the present work, we believe the synthesis of anatase titanium dioxide NPs with size in the range of 5–10 nm. Colloidal solution of NPs produced with ablation of iron rod in double-distilled water has wide hump ranging from 220 to 400 nm with long tail upto 700 nm. Observed hump is the characteristic of FeO NPs, while long tail is due to the presence of defect in iron oxide lattice as a result of non-equilibrium processing. The colloidal solution of NPs produced after 60 min ablation of Fe rod in the colloidal solution of $TiO_2$ NPs has absorption hump around 350 nm

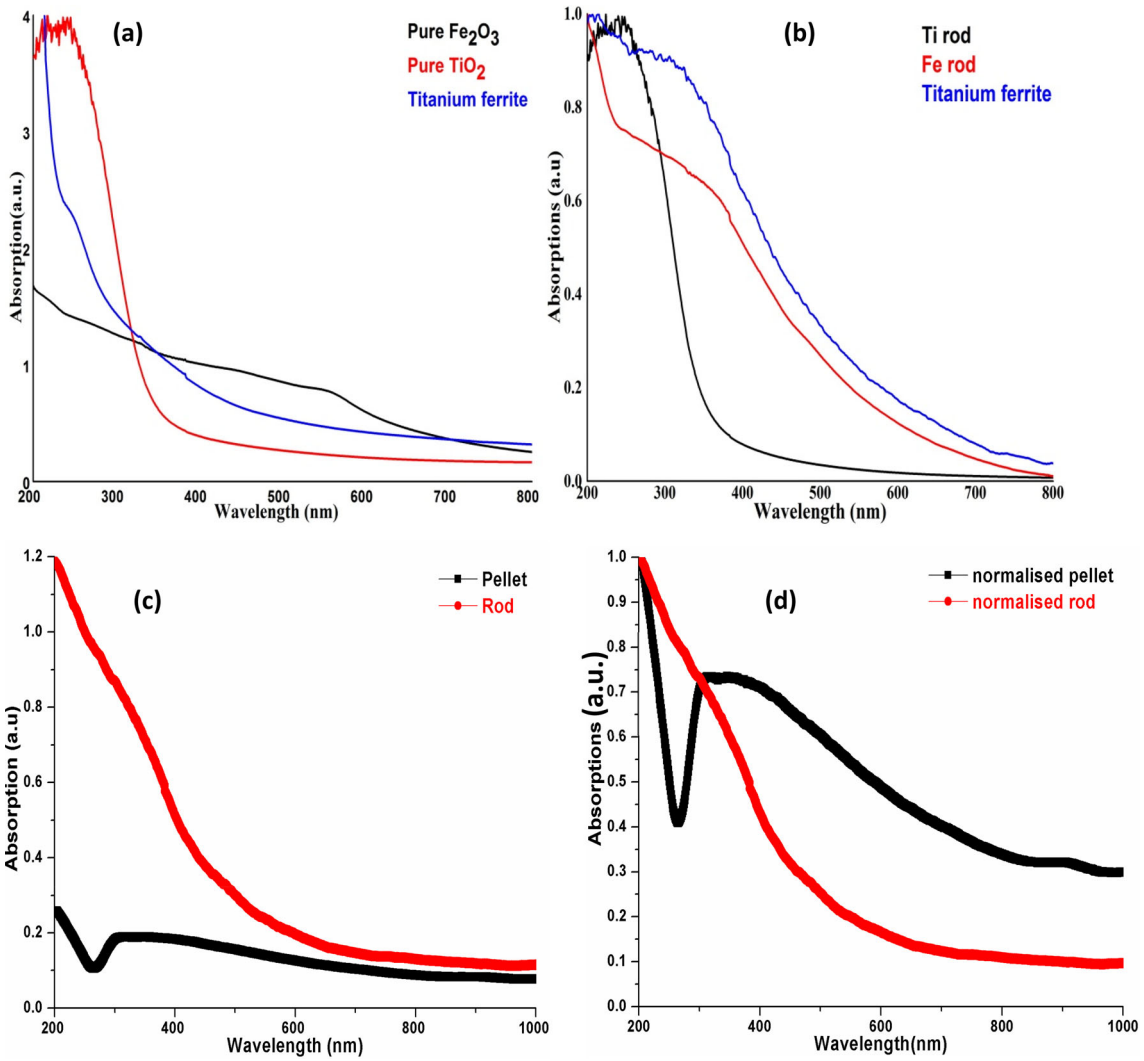


**Figure 4.** UV–Vis spectra of titanium ferrite nanoparticles obtained from ablation of targets.

(blue curve), in between the absorption hump of FeO (red curve) and absorption peak of $TiO_2$ (black curve), showing synthesis of titanium ferrite NPs. Optical absorption data supports our XRD results. Absorbance at 200 nm, generally determines density of NPs in the solution. Ceramic target was ablated for 60 min, while rods were ablated for 120 min (60 min for titanium followed by 60 min iron) under the same experimental conditions. Generally, rate of ablation in the liquid decreases with time due to deleterious effect of NPs present in the solution. Comparative optical absorption data, in original (figure 4c) and normalized (figure 4d) forms of NPs produced after PLA of ceramic (black curve) and metallic targets (red curve) show that optical absorbance of colloidal solution obtained from rod is more than five times larger than that produced from ceramic target, while time of ablation was only two times larger. Higher absorbance for solution produced with rod shows a higher rate of material removal and hence, a higher rate of NPs production when metallic rods are used as targets.

### 3.4 *Vibrational characterizations of titanium ferrite NPs using FTIR and Raman spectroscopic techniques*

FTIR spectroscopy is a label-free, non-destructive analytical technique which can be used to study vibrational frequency between cation and anion to determine crystalline structure of NPs and presence of functional molecules on its surface. It gives the identification of the functional group associated with the chemical present in the sample under investigation. High resolution FTIR spectra of titanium ferrite NPs produced with the ablation of metallic rods and ceramic pellet are shown in figure 5 along with FTIR spectra of their corresponding targets for reference. Titanium and iron are highly active metals and react with hydroxyl ions generated at plasma-medium interface to produce their oxide NPs in the solution and formation of a thin layer of oxides on the surface of rods. FTIR measurements of iron (figure 5a; red curve) and titanium (figure 5a; black curve) rods, used for ablation, show vibrational modes of Fe–O and Ti–O, respectively. Vibration peak around 529 $cm^{-1}$ is assigned to the stretching vibration of Ti–O bond. A close resemblance of FTIR spectrum of oxide layer on Ti surface with FTIR spectrum of bulk $TiO_2$ powder (figure 5b, red curve) shows synthesis of $TiO_2$ NPs in the solution and at the target surface as a result of LPPs of titanium with water plasma at the interface. Similarly, FTIR investigation for the surface chemistry of iron rod shows the presence of absorption peaks at 532 and 584 $cm^{-1}$ corresponding to vibrational stretching modes of Fe–O bond. In spinel ferrites, stretching vibration of tetrahedral and octahedral groups has absorption bands around 550 and 350 $cm^{-1}$, respectively [47]. FTIR spectrum of NPs produced from pellet has clear absorption hump around 550 $cm^{-1}$, while it is hidden under the wide peak width of Ti–O/Fe–O vibrational band. From these observations, one can say that NPs produced with PLA of pellet target has higher relative composition of spinel ferrite.

Raman spectroscopy is a powerful non-destructive vibrational spectroscopic technique for investigation of crystalline structure of NPs. Figure 5 shows the Raman spectra of titanium ferrite NPs produced via LP-PLA of ceramic pellet target and rods. Spinel ferrites have five Raman active, $A_{1g}$, $E_g$ and $3T_{2g}$ modes associated to the motion of A-site and B-site cations and O ions [48]. Furthermore, the $T_{2g}$ mode relates to the asymmetric motion of tetrahedral and octahedral cations with respective oxygen anions, the $E_g$ mode is due to symmetric bending of the oxygen anion, and $A_{1g}$ Raman mode is associated with symmetric stretching of oxygen anions [47]. From figure 6, it can be seen that the NP samples produced from both routes show Raman modes at ~230, ~295, ~410, ~500, ~613 and ~660 $cm^{-1}$. The lower frequency (~230,

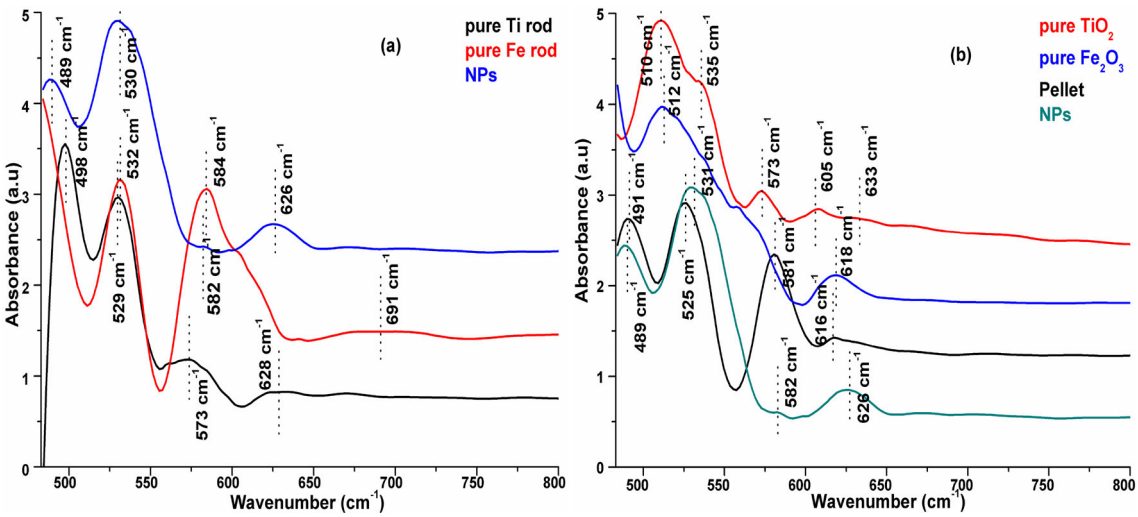


**Figure 5.** ATR-FTIR spectra of titanium ferrite nanoparticles synthesized by ablation of (**a**) rods and (**b**) pellets.

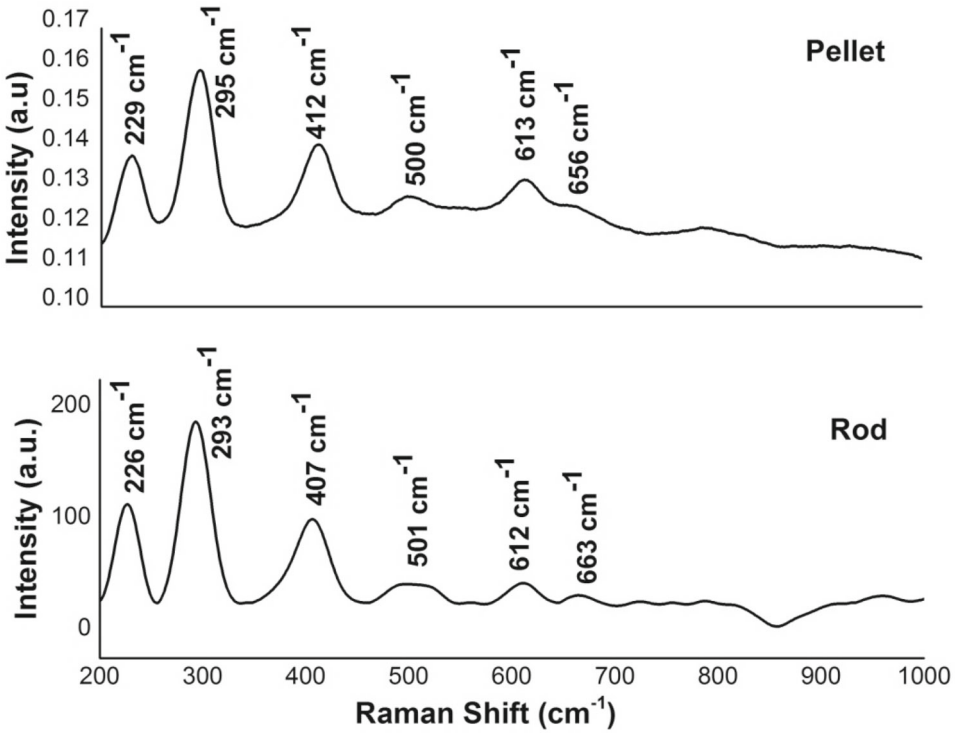


**Figure 6.** Raman spectra of titanium ferrite nanoparticles synthesized by the ablation of pellets and rod targets.

~295, ~410 and ~500 $cm^{-1}$) Raman vibrational modes are assigned to $T_{2g}$ and $E_g$ Raman modes associated to the vibration of the spinel structure. The higher frequency (~613 and ~660 $cm^{-1}$) vibrational modes are assigned to $A_{1g}$ (1) and $A_{1g}$ (2) modes related to the stretching vibrations of the Ti–O and Fe–O bonds in tetrahedral sites.

### 3.5 *Magnetic properties of titanium ferrite NPs produced via two approaches*

Variations in magnetization (emu $g^{-1}$) as a function of applied magnetic field (*M–H* curve) for titanium ferrite NPs produced via two target approaches are shown in figure 7. The values of coercivity ($H_c$), saturation magnetization ($M_s$) and remanence magnetization ($M_r$) for two samples are extracted from corresponding *M–H* curves and are presented in table 2. It is interesting to note that the values of $M_s$, $M_r$ and $H_c$ are 2–3 times higher for NPs produced with pellet as compared to that produced from rods under the same experimental conditions. Higher ferromagnetism for titanium ferrite NPs produced with ceramic pellet is related to its synthesis mechanism that leads to the formation of better-quality spinel ferrite structure with less surface defect. Higher ferromagnetism in smaller-sized NPs produced with PLA of ceramic pellets shows that the surface atoms/defects play positively in the generation of unpaired spin responsible for long-range ferromagnetism [49].

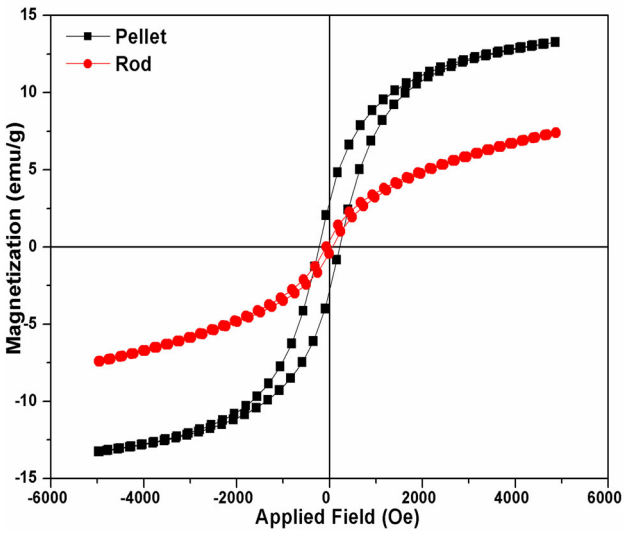


**Figure 7.** *M–H* loop of titanium ferrite nanoparticles synthesized from two different targets.

### 3.6 *Synthesis mechanism*

Pulsed laser beam irradiates metal surface at solid–liquid interface through transparent liquids and produces LPPs under liquid confinement. LPPs interact and ionize with surrounding liquid to produce PIPs having anionic species from liquid medium [23,46]. Strong physical confinement of LPPs between target and surrounding liquid increases its temperature, pressure, density and hence, kinetic energy of

**Table 2.** Represents magnetic parameters of titanium ferrite NPs.

| Target | Crystal size (nm) | Band gap (eV) | $M_s$ (emu $g^{-1}$) | $M_r$ (emu $g^{-1}$) | $H_c$ (Oe) |
|---|---|---|---|---|---|
| Pellet | 23.53 | 2.50 | 13.27 | 2.86 | 221.92 |
| Rod | 50.37 | 2.55 | 7.28 | 0.36 | 53.17 |

ions and neutrals [50]. Constituents of LPPs and PIPs expand toward each other with high velocity and make reaction at interface under thermal non-equilibrium. LPPs and PIPs having cations from target materials and anions from liquid, react at interface to produce metal hydroxide (for water) followed by its oxides with the following reactions:

$$H_2O \rightarrow H^+ + OH^-, \quad (1)$$

$$Fe^{2+} + 2OH^- \rightarrow Fe(OH)_2, \quad (2)$$

$$Fe(OH)_2 + 2Fe(OH)_3 \rightarrow Fe_3O_4 + 4H_2O, \quad (3)$$

$$Ti^{2+} + 2OH^- \rightarrow Ti(OH)_2, \quad (4)$$

$$Fe_3O_4 + 2TiO_2 \rightarrow FeTiO_3 + Fe_2TiO_5. \quad (5)$$

## 4. Conclusions and future perspectives

Titanium ferrite NPs are synthesized using LP-PLA technique with two different lines of approaches for targets: the first target is the pellet made from the mixture of oxides of iron and titanium, while the second target is iron and titanium metal rods. In the second approach of metal rods, the titanium rod was first ablated in double-distilled water and then, as-obtained colloidal solution of NPs is used as a medium for the ablation of iron rod. NPs produced from both routes have multiple phases of titanium ferrite. Product obtained from LP-PLA of ceramic pellet has titanium ferrite phases of $TiFe_2O_4$, $Ti_3Fe_3O$, $TiFe_2O_5$ and $Fe_{0.23}(Fe_{1.95}Ti_{0.42})O_4$ with abundance of spinel ferrite structure. In contrast, sample produced with sequential ablation of rods has $Ti_2Fe_2O_7$ (landauite), $TiFe_2O_5$ (pseudobrookite), $(Ti_{0.81}Fe_{0.13})O_{1.92}$ and iron-deficient wuestile phase of iron oxide $(Fe_{0.87}O)_{10}$. The crystalline size of titanium ferrite NPs obtained from the ablation of pellet is $\sim$23 nm, while that produced with the PLA of rods is $\sim$50 nm. FTIR and Raman investigation results for vibrational modes show that NPs produced with PLA of ceramic pellet has higher quality of spinel ferrite as compared to that produced from rods. Due to higher abundance of spinel ferrite, the values of coercivity ($H_c$), saturation magnetization ($M_s$) and remanence magnetization ($M_r$) of sample produced from pellet are 2–3 times higher than that produced from rods under the same experimental conditions. The results of present research demonstrate collision and intermixing of plasmas from two different species and can be used to produce bimetallic NPs of other metals.

## Acknowledgements

We are thankful to BRNS-DAE, UGC and DST, New Delhi, for providing financial assistance to create the ATR-FTIR and confocal micro-Raman spectroscopy facility under UGC–CAS and FIST program to the Department of Physics, University of Allahabad, Prayagraj, India.

## References

[1] Singh S C, Li H, Yao C, Zhan Z, Yu W, Yu Z *et al* 2018 *Nano Energy* **51** 774
[2] Devolder T, Tahmasebi T, Eimer S, Hauet T and Andrieu S 2013 *Appl. Phys. Lett.* **103** 242410
[3] Singh S C and Gopal R 2008 *J. Phys. Chem. C* **112** 2812
[4] Qi X, Zhang M, Zhang X, Gu Y, Zhu H, Yang W *et al* 2017 *RSC Adv.* **7** 51801
[5] Singh S C, Peng Y, Rutledge J and Guo C 2019 *ACS Appl. Electron. Mater.* **1** 1169
[6] Li L, Niu R and Zhang Y 2018 *RSC Adv.* **8** 12428
[7] Wu K, Li J and Zhang C 2019 *Ceram. Int.* **45** 11143
[8] Arimi A, Megatif L, Granone L I, Dillert R and Bahnemann D W 2018 *J. Photochem. Photobiol. A: Chem.* **366** 118
[9] Mahalakshmi S, Jayasri R, Nithiyanatham S, Swetha S and Santhi K 2019 *Appl. Surf. Sci.* **494** 51
[10] Martineze Vargas S, Martínez A I, Hernandez-Beteta E E, Mijangose-Ricardez O F, Vazquez-Hipolito V, Patino-Carachure C *et al* 2018 *J. Mol. Struct*. **1154** 524
[11] Martínez-Rodríguez N L, Tavárez S and González-Sánchez Z I 2019 *Toxicol. In Vitro* **57** 54
[12] Adebiyi B M, Duraia E S M and Beall G W 2019 *J. Magn. Magn. Mater.* **489** 165401
[13] Carotta M C, Ferroni M, Gnani D, Guidi V, Merli M, Martinelli G *et al* 1999 *Sens. Actuators B* **58** 310
[14] Jaroenworaluck A, Sunsaneeyametha W, Kosachan N and Stevens R 2006 *Surf. Interface Anal.* **38** 473
[15] Linsebigler A L, Lu G and Yates Jr J T 1995 *Chem. Rev.* **95** 735
[16] Zhang L, Kanki T, Sano N and Toyoda A 2003 *Sep. Purif. Technol.* **31** 105
[17] Sun S, Murray C B, Weller D, Folks L and Moser A 2000 *Science* **287** 1989
[18] Kim T H, Jang E Y, Lee N J, Choi D J, Lee K-J, Jang J-T *et al* 2009 *Nano Lett*. **9** 2229
[19] Tromsdorf U I, Bruns O T, Salmen S C, Beisiegel U and Weller H 2009 *Nano Lett*. **9** 4434
[20] Laurent S, Forge D, Port M, Roch A, Robic C, Elst L V *et al* 2008 *Chem. Rev.* **108** 2064
[21] Laurent S, Dutz S, Häfeli U O and Mahmoudi M 2011 *Adv. Colloid Interface Sci.* **166** 8

[22] Chirita M and Grozescu I 2009 *Chem. Bull.* **54** 1
[23] Singh S C, Zeng H, Yang S, Cai W, Hong M, Chen G *et al* 2012 in *Nanomaterials: processing and characterization with lasers* (Germany: John Wiley & Sons) Chap 6, p 317 ISBN: 978-0-470-17795-2
[24] Anikin K V, Melnik N N, Simakin A V, Shafeev G A, Voronov V V and Vitukhnovsky A G 2002 *Chem. Phys. Lett.* **366** 357
[25] Singh S C and Gopal R 2010 *J. Phys. Chem. C* **114** 9277
[26] Singh S C, Swarnkar R K and Gopal R 2009 *J. Nanopart. Res.* **11** 1831
[27] Semaltianos N G, Logothetidis S, Perrie W, Romani S, Potter R J, Sharp M *et al* 2009 *Appl. Phys. A* **94** 641
[28] Semaltianos N G, Logothetidis S, Perrie W, Romani S, Potter R J, Sharp M *et al* 2009 *Appl. Phys. Lett.* **95** 033302
[29] Luches A and Aaron Peled 2005 *Appl. Surf. Sci.* **248** 209
[30] Neumeister A, Jakobi J, Rehbock C, Moysig J and Barcikowski S 2014 *Phys. Chem. Chem. Phys.* **16** 23671
[31] Zhang J, Oko D N, Garbarino S, Imbeault R, Chaker M, Tavares A C *et al* 2012 *J. Phys. Chem. C* **116** 13413
[32] Malviya K D and Chattopadhyay K 2014 *J. Phys. Chem. C* **118** 13228
[33] Amendola V, Meneghetti M, Bakr O M, Riello P, Polizzi S, Anjum D H *et al* 2013 *Nanoscale* **5** 5611
[34] Sree Satya Bharati M, Byram C and Soma V R 2018 *Front. Phys.* **6** 28
[35] Singh S C and Gopal R 2008 *Physica E* **40** 724
[36] Singh S C 2011 *J. Nanopart. Res.* **13** 4143
[37] Streubel R, Barcikowski S and Gökce B 2016 *Opt. Lett.* **41** 1486
[38] Streubel R, Bendt G and Gökce B 2016 *Nanotechnology* **27** 205602
[39] Singh S C, Zeng H, Guo C and Cai W (eds) 2012 *Nanomaterials: processing and characterization with lasers* (Germany: John Wiley & Sons) ISBN: 978-0-470-17795-2
[40] Shukla A, Singh S C, Pandey B K, Uttam K N, Shah J, Kotnala R K *et al* 2015 *Adv. Mater. Lett.* **12** 1066
[41] Singh S C, Swarnkar R K and Gopal R 2009 *J. Nanosci. Nanotech.* **9** 5367
[42] Mullen E K and Mccallum I S 2013 *Am. Mineral.* **98** 417
[43] Seitz G, Penin N, Decoux L, Wattiaux A, Duttine M and Gaudon M 2016 *Inorg. Chem.* **55** 2499
[44] Singh S C, Mishra S K, Srivastava R K and Gopal R 2010 *J. Phys. Chem. C* **114** 17374
[45] Shukla A, Bhardwaj A K, Singh S C, Uttam K N, Gautam N, Himanshu A K *et al* 2018 *J. Appl. Phys.* **123** 161411
[46] Zeng H, Du X-W, Singh S C, Kulinich S A, Yang S, He J *et al* 2012 *Adv. Funct. Mater.* **22** 1333
[47] Choi Y I, Kim Y-I, Cho D W, Kang J-S, Leung K T and Sohn Y 2015 *RSC Adv.* **5** 79624
[48] Chandramohan P, Srinivasan M P, Velmurugan S and Narasimhan S V 2011 *J. Solid State Chem.* **184** 89
[49] Singh S C, Kotnala R K and Gopal R 2015 *J. Appl. Phys.* **118** 64305
[50] Singh S C, Fallon C, Hayden P, Mujawar M, Yeates P and Costello J T 2014 *Phys. Plasmas* **21** 093113